SAND99-0499C

A microelectromechanical high-density energy storage / rapid release system

M. Steven Rodgers, Jim J. Allen, Kent D. Meeks, Brian D. Jensen, and Sam L. Miller

Intelligent Micromachine Department, Sandia National Laboratories
Mail Stop 1080 P. O. Box 5800
Albuquerque, NM 87185-1080
http://www.mdl.sandia.gov/Micromachine

ABSTRACT

One highly desirable characteristic of electrostatically driven microelectromechanical systems (MEMS) is that they consume very little power. The corresponding drawback is that the force they produce may be inadequate for many applications. It has previously been demonstrated that gear reduction units or microtransmissions can substantially increase the torque generated by microengines [1,2]. Operating speed, however, is also reduced by the transmission gear ratio. Some applications require both high speed and high force. If this output is only required for a limited period of time, then energy could be stored in a mechanical system and rapidly released upon demand. We have designed, fabricated, and demonstrated a high-density energy storage / rapid release system that accomplishes this task. Built using a 5-level surface micromachining technology [3], the assembly closely resembles a medieval crossbow. Energy releases on the order of tens of nanojoules have already been demonstrated, and significantly higher energy systems are under development.

Keywords: microengine, microtranmission, microelectromechanical energy storage

1. INTRODUCTION

Micromachined electrostatic comb drives are generally considered to be low power devices producing only a few tens of micronewtons of force [4,5]. Although their thermal counterparts may be able to increase this value by 1 to 2 orders of magnitude [6], actuation speed is limited. Therefore, electrically driven microelectromechanical systems have not been considered to be suitable candidates for applications requiring powerful transient releases of energy. Recent advances in multi-level surface micromachined actuation and energy storage systems, however, are changing this perception and making it possible to consider MEMS as potential candidates for many new high energy applications such as initiators, gene injectors, and nanosatellite thrusters.

The high-density energy storage and rapid release system that was developed to demonstrate this actually evolved from structures that were originally designed to evaluate the performance of the actuation components used in the complex microelectromechanical system shown in figure 1. This is a research prototype that demonstrated the level of complexity required for advanced weapon safety systems could be realized in a surface micromachined technology. Detailed information about this system has been previously published [7,8], so only a brief description is given here. As fabricated, the chain of gears that connects the mirror to the mirror control engine is interrupted at the point indicated. This prevents the engine from driving the mirror to a useful operating position until two additional coupling gears are inserted, which occurs automatically after the correct 24-bit electrical code has been applied to the pin-in-maze discriminator (locking device) shown on the right half of the figure. The maze track and mirror control engines are mirror copies of each other, and both utilize the same modular transmission assemblies to increase torque and drive their respective loads. This was the first system ever specifically designed for and fabricated in a 5-level surface micromachined technology [3], and it proved to be a very successful demonstration. Being the first of its kind, no performance data was available for any of the components, so the actuation systems were conservatively designed to help ensure success. This paper provides a detailed description of these components, the assemblies that were envision to determine their performance, and the enhancements that were made to realize the high-density energy storage and rapid release mechanism.

DISCLAIMER

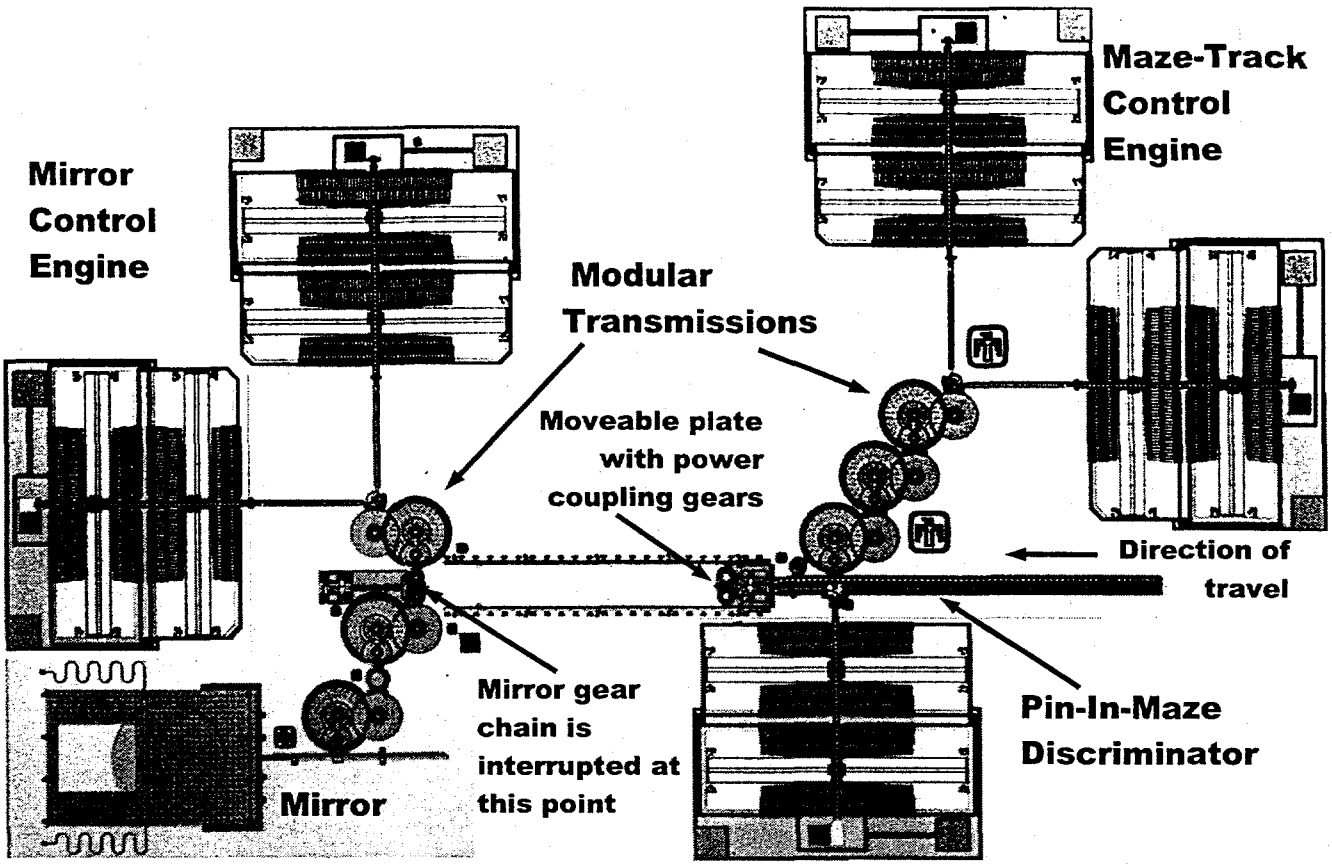

Figure 1. Optical micrograph of the 5-level surface micromachined safety system. Evaluation of the core actuation components employed in this assembly led to the development of the high-density energy storage/rapid release mechanism.

2. FABRICATION TECHNOLOGY

All of the devices presented here were fabricated in a state-of-the-art 5-level surface micromachined technlogy known as SUMMiT-V (Sandia Ultra-planar Multi-level MEMS Technology V) [7]. This process, shown in figure 2, defines 4 mechanical layers of polysilicon referred to as poly1, poly2, poly3, and poly4 that are fabricated above a poly0 electrical interconnect and ground plane layer [2]. Poly0 is 0.3 μm thick; poly1 is 1.0 μm, poly 2 is 1.5 μm, and both poly3 and poly4 are 2.25 μm. All films except poly1 and poly2 are separated by 2-μm thick depositions of sacrificial oxide. A 0.5-μm sacrificial oxide between poly1 and poly2 typically defines the clearance between close mating parts such as hubs and hinges. This entire stack is built on a single crystal substrate with a dielectric foundation of 0.8 μm of nitride over 0.63 μm of oxide. Seventeen drawing layers are combined to generate the 14 photolithographic masks used to pattern these films during a 240-step fabrication sequence.

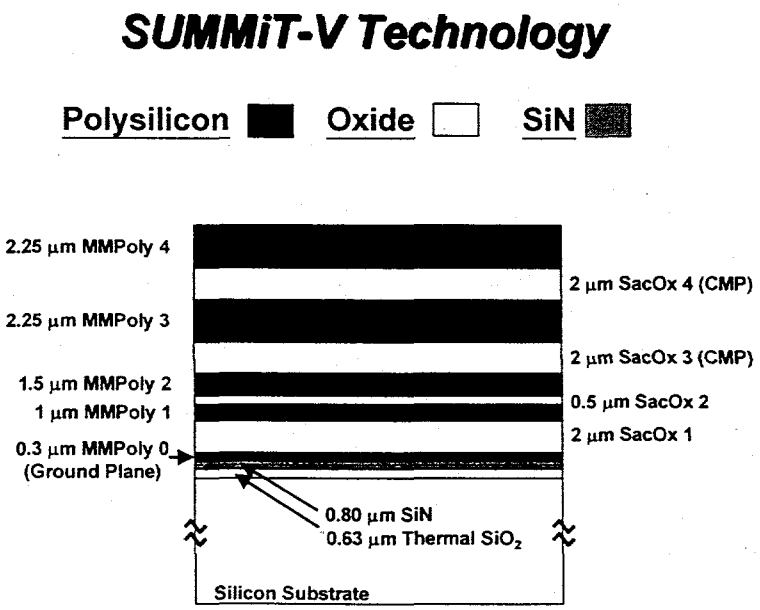

Figure 2. SUMMiT-V fabrication stack. Note that the upper two sacrificial oxide films are planarized by chemical mechanical polishing (CMP).

3. ADVANCED MICROENGINE

The electrostatically driven microengine, which is based on a pinion gear that is coupled with linkage arms to 2 orthogonal comb drives as shown in figure 3A [9], has become the actuation system of choice for most of the microelectromechanical systems fabricated at Sandia National Laboratories. This is largely due to the years of research and continuous improvements that have turned this device into a dependable actuation system [7,10,11,12,13]. With the 5-level technology, it was possible to advance the microengine even further. For comb drives the output force is proportional to the thickness of the fingers, and the out of plane compliance varies inversely with the cube of the spring thickness. By utilizing all of the available layers of polysilicon for the comb fingers (figure 3B), drive force was increased nearly 50% above what was obtainable with the previous designs in the standard 4-level SUMMiT process [2]. More significantly, however, is that by also doing the same thing for the suspension springs (figure 3C), the "Z" axis or out of plane stiffness is approximately 100 times greater than first generation devices [7]. This dramatically increases robustness, and significantly increases yield by reducing the chance that surface tension during the release process will pull the comb assembly down to the substrate and leave it adhered. The 5-level technology also allows investigation of advanced linkages such as the one shown in figure 3D.

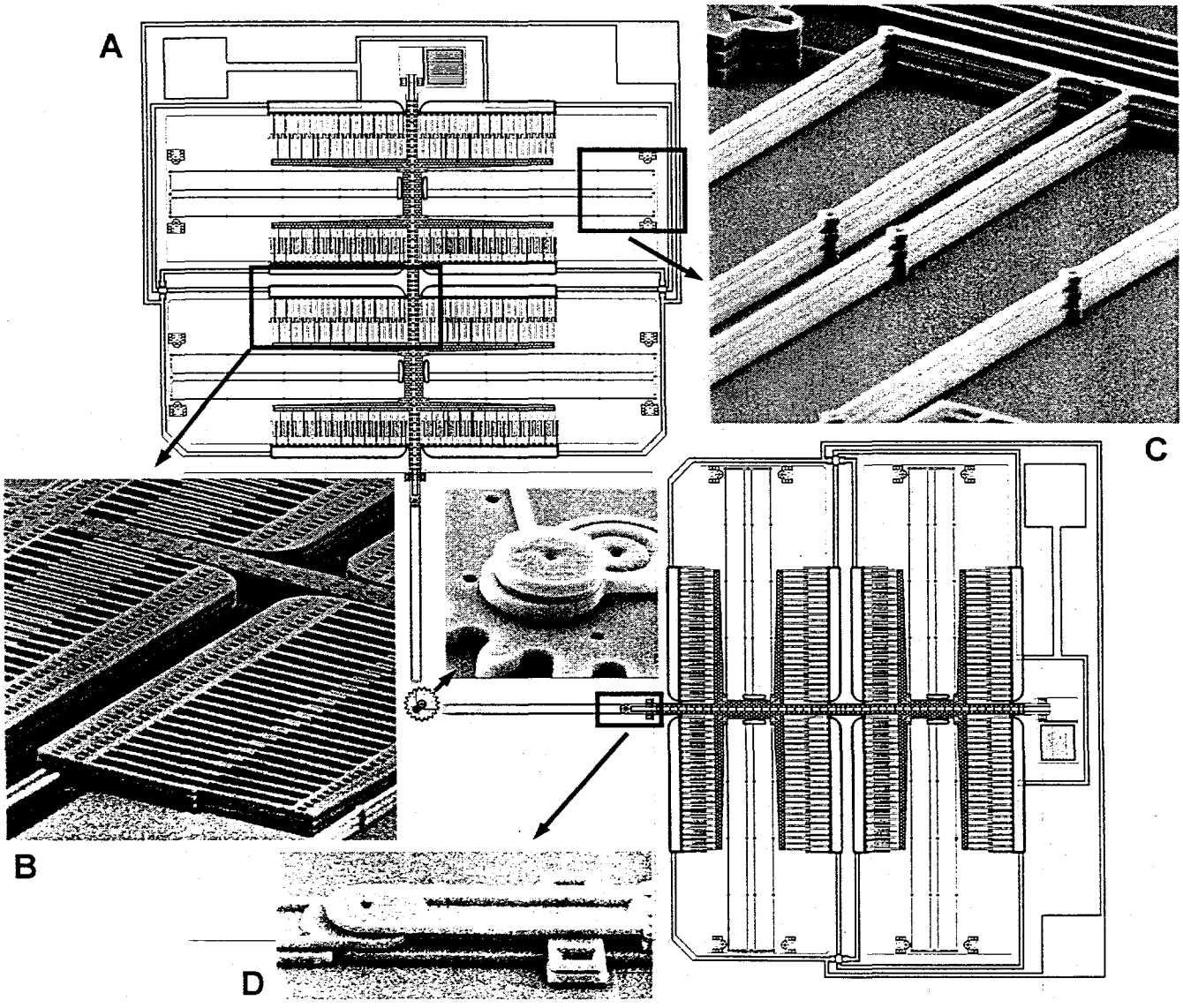

Figure 3. A CAD drawing of the 5-level microengine and Scanning Electron Microscope (SEM) images of some of its components.

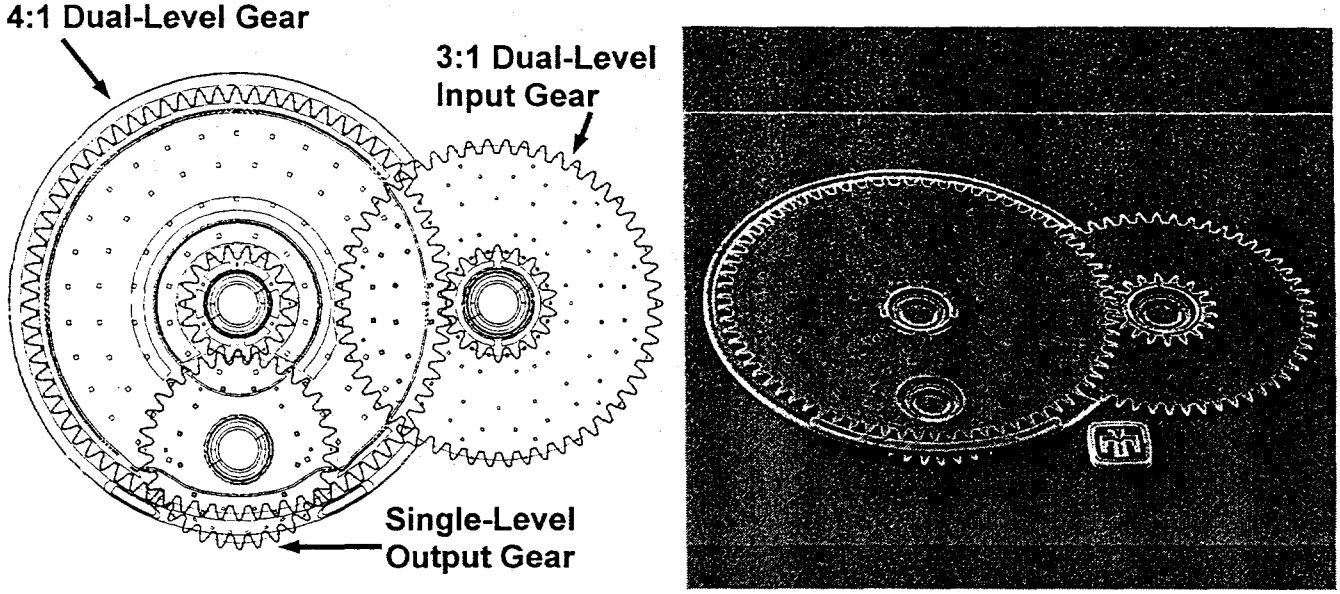

Figure 4. A CAD drawing of the 12:1 modular transmission assembly is shown on the left, and a SEM image of the fabricated device is shown on the right. The offset hole in the largest gear exposes the output gear hub and serves as an indicator for easily determining rotational position.

4. TORQUE MULTIPLICATION

The energy storage system utilizes gear reduction assemblies to dramatically increase the torque from the microengine. Microelectromechanical gear reduction units or microtransmissions were first used in 1996 as a means to create enough torque to demonstrate a fully self-actuated MEMS mirror [12]. This was accomplished without using any additional assistance to initially elevate the mirror from its fabricated position. Nonetheless, the first microtransmission was application specific and in many cases required extensive modification to be incorporated into other systems. Therefore, the modular transmission shown in figure 4 was developed as a drop in device that could easily be employed in numerous designs [7]. The first component of this assembly is a dual-level input gear having 54 teeth on the lower gear and 18 teeth on the upper yielding a 3:1 gear reduction ratio. The second dual-level component has 72 teeth on the upper gear and 18 on the lower to generate a 4:1 reduction ratio. This yields an overall gear reduction ratio of exactly 12:1. Gear reduction assemblies used in power trains typically use gears machined with prime numbers of teeth to reduce wear [14]. However, wear has not been observed to be an issue for micromachined teeth, and the integer ratio makes it easier to synchronize a stop action strobe to the electrical drive signals for analysis. To make these assemblies cascadable, a 32 tooth single-level coupling gear is fabricated beneath the 72 tooth gear and mated to its 18 tooth counterpart. This provides for a modular approach when designing with these assemblies, and they are used in the layout process much like one would use clipart. The coupling gear of the final stage serves as the output. The SEM image in figure 5 illustrates how these transmissions can be coupled together and to the microengine drive pinion.

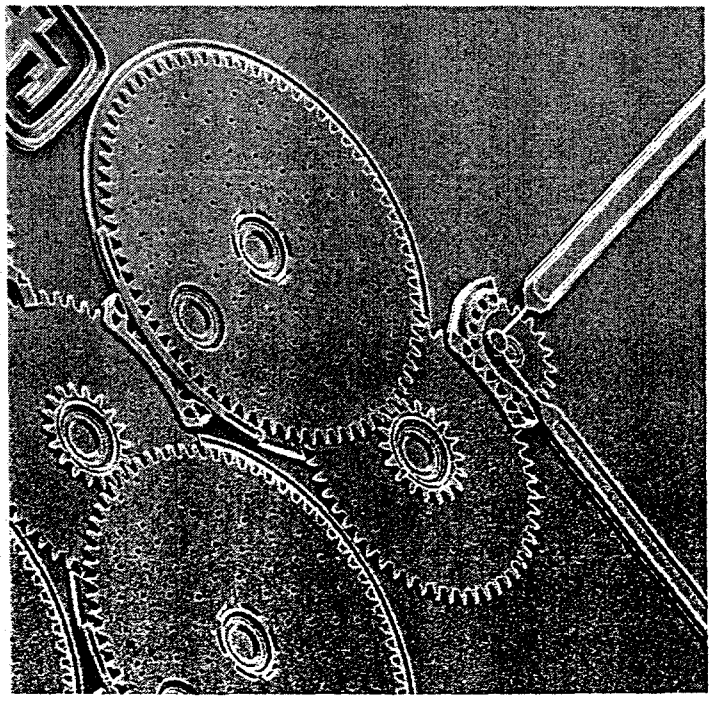

Figure 5. Angled SEM image of two cascaded modular transmission assemblies driven by a microengine pinion gear. Mirroring of the transmissions only requires a single step during the layout process.

5. SYSTEM DESIGN

5.1 Energy Storage

As stated earlier, the energy storage system evolved from the need to create structures to evaluate how much torque could actually be generated with the new 5-level microengine and transmission assemblies [7]. One of the ways to do this is to have the output gear of the final transmission stage pull on a rack that deflects one or more cantilever beams, and then use the beam geometry and the material properties of polysilicon to calculate the applied force. Several designs based upon this approach were considered before settling on the one shown below in figure 6. To increase structural stability, several narrow cantilever beams were stacked on top of each other and then placed on both sides of a central shaft. The resulting assembly closely resembles a medieval crossbow. Instead of a single bow, however, 18 cantilever beams are paired together to create a system that has a total of 9 bows with a single central shaft taking the place of an arrow. Significant potential energy is stored in these beams as a microengine with a 20,000:1 (actually 20736:1) gear reduction assembly drives a rack that pulls on the central shaft. The gear assembly is defined by a chain of four 12:1 modular transmissions.

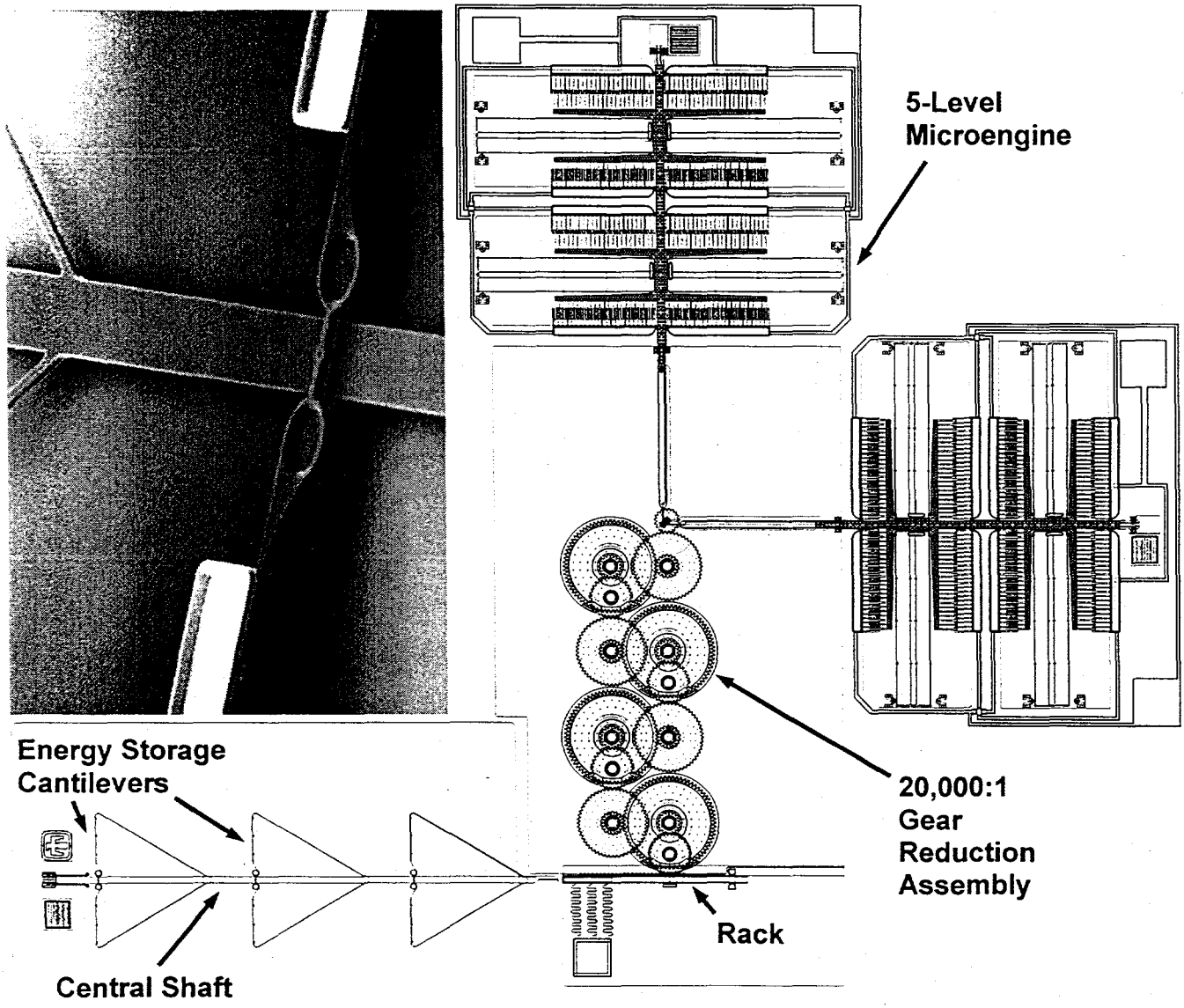

Figure 6. A CAD drawing of the high density energy storage system with an SEM image of the multi-level cantilever beams that comprise its "bows".

5.2 Energy Release

The central shaft is connected to the rack through a thin polysilicon filament as shown in figure 7. Also connected to this rack are three very compliant springs that have a combined cross sectional area much larger than that of the filament itself. The other end of these springs is connected to a bond pad. After energizing the bows, an electrical pulse is applied to this pad. Current flows through the three compliant springs, through the filament, and then to ground through the tethers that connect the central shaft to the cantilever beams. If enough voltage and current is applied, the filament blows, releasing the shaft and allowing the potential energy stored in the beams to be converted into kinetic energy that can be directed to a mechanical load. Loads placed in close proximity to the end of the central shaft could be impacted directly by this shaft. In this configuration, however, the central shaft impacts a small projectile (refer again to figure 7) that can strike a more remote target.

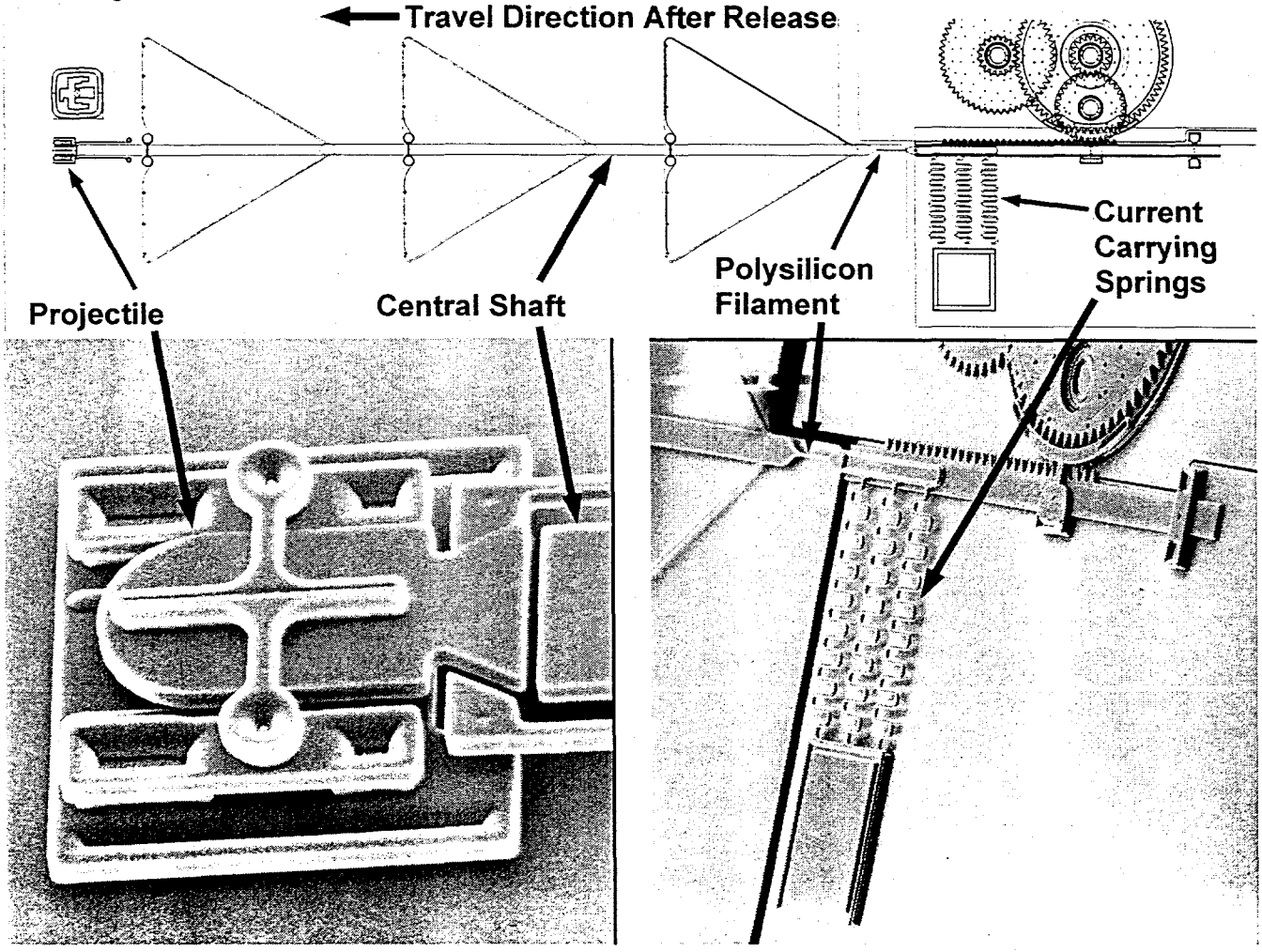

Figure 7. The filament that connects the central shaft to the rack is shown on the right. Also shown are the compliant electrical connections. On the left is the small projectile that is rapidly ejected by impact from the central shaft when the filament is blown. An enlarged view of the lower section of the drawing used in figure 6 is used to establish component location.

6. ANALYSIS

The energy storage of this device may be estimated using kinematic modeling. The storage of one flexible beam will be studied, with simple multiplication allowing generalization to multiple beams. Compliant mechanism theory [15,16] can be used to model the flexible beam shown in Figure 8A as two rigid beams joined by a pin joint, with a torsional spring representing the beam stiffness, as shown in Figure 8B. This model assumes that the beam is loaded purely with a force,

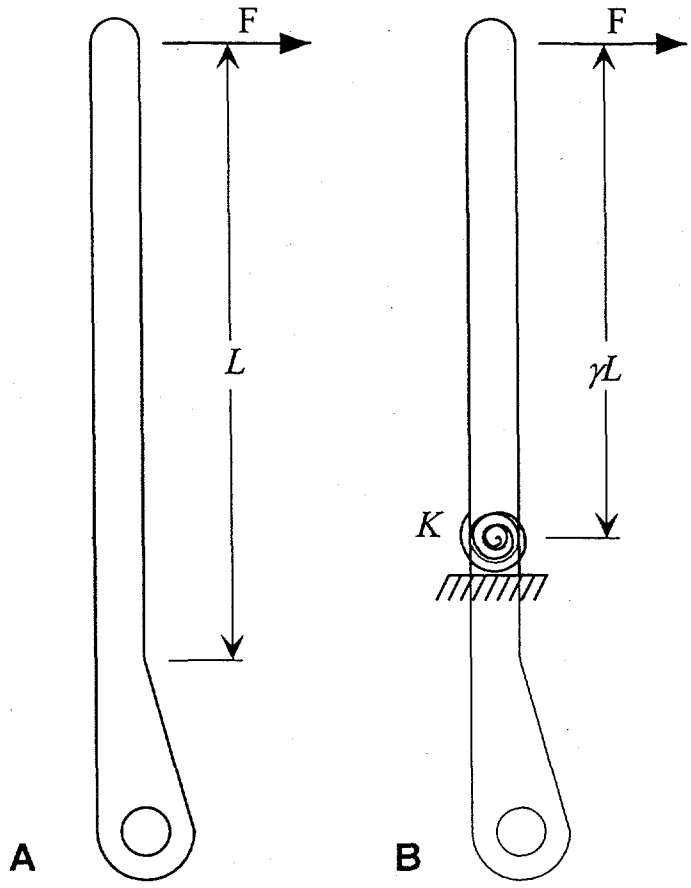

Figure 8. Each flexible beam "A" may be modeled using compliant mechanisms theory as two rigid segments, one fixed and the other rotating "B". A torsional spring with spring constant K represents the beam's stiffness.

F, at its end, which is a reasonable assumption, as the thin tether connecting the beam to the shuttle transfers negligible moment loads. The rotating link in this model is termed the "pseudo-rigid beam", and its length is γL, where γ is a constant known as the characteristic radius factor, whose value is determined by the direction of the load. The torsional spring has a constant spring stiffness, given by:

$$K = \gamma K_\Theta \frac{EI}{L} \qquad (1)$$

where K_Θ is another constant called the stiffness coefficient, also determined by the direction of loading. In this equation, E represents Young's modulus, I is the area moment of inertia of the beam cross-section, and L is the length of the flexible beam. Over a wide range of load directions, γ may be approximated as 0.85, and K_Θ as 2.65 [16].

This flexible beam model may be incorporated in a larger kinematic model by assuming that the thin tether stores negligible energy, so that it acts as a tensile member only, as shown in the model in Figure 9. The shuttle may then be modeled as a slider element, also shown in the figure. The energy storage in this mechanism is equal to:

$$V = \frac{1}{2} K \Theta^2 \qquad (2)$$

where K is the torsional spring constant given in Equation (1) and Θ is the angle made by the pseudo-rigid beam with its original vertical position. As a force is applied to the slider shown in Figure 2, the mechanism deflects a distance δ, which causes Θ to increase, increasing the energy storage. A sample deflection is illustrated in the figure. For a given δ, Θ may be found by solving the simultaneous equations:

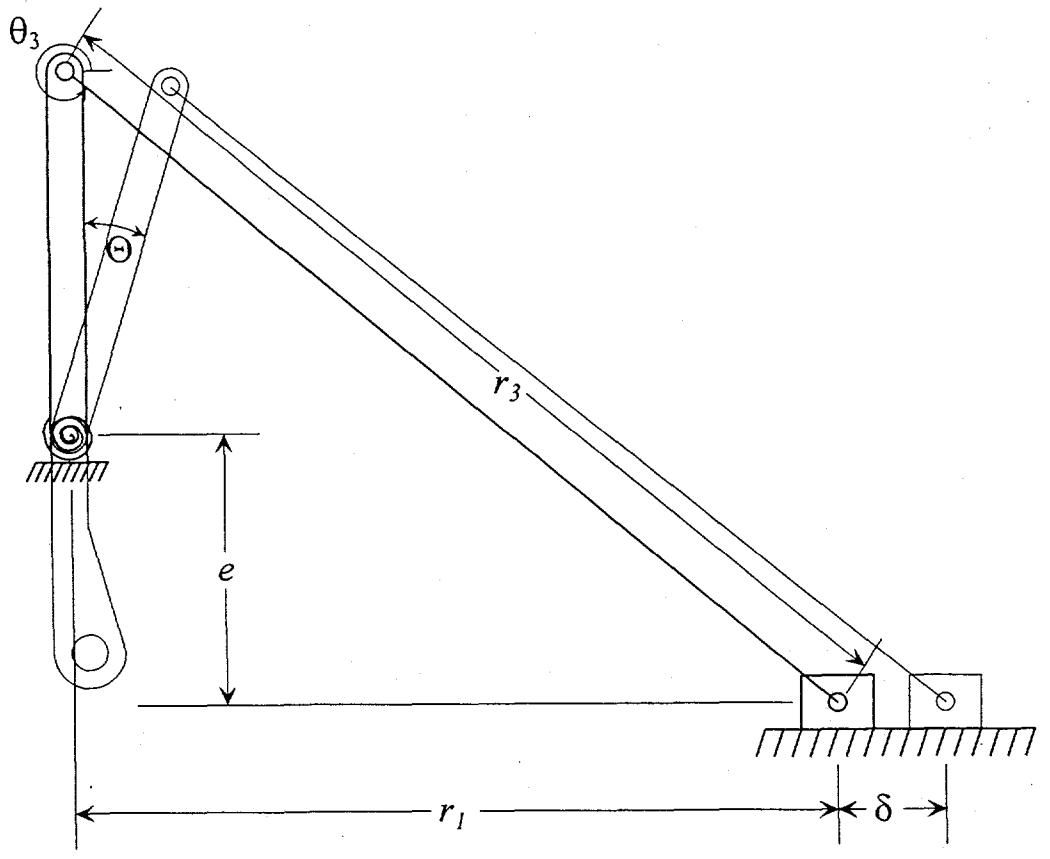

Figure 9. The kinematic model of the beam and shuttle.

$$\delta = \gamma L \sin \Theta + r_3 \cos \theta_3 - r_1 \qquad (3)$$

and

$$\theta_3 = -\sin^{-1}\left(\frac{e + \gamma L \cos \Theta}{r_3}\right) \qquad (4)$$

where the various mechanism parameters are defined in Figure 9. Finally, the force which must be applied to the shuttle is given by:

$$F = \frac{K\Theta \cos \theta_3}{\gamma L \cos(\Theta + \theta_3)} \qquad (5)$$

For the energy storage device presented here, there are a total of six sets of the multi-level beams like the one analyzed above. The parameters which appear in Equations (1) through (5) are shown in Table 1 for this device. Using these parameters, the equations were solved, resulting in the graphs shown in Figure 10 and Figure 11. In these graphs, the force and energy are given, respectively, as a function of δ, the deflection of the shuttle. For a fifty micron deflection, which is approximately the deflection attained during actual testing of the device, the graphs show that the device stores about 19 nJ of energy, with a force applied to the shuttle of about 735 μN. Assuming negligible losses and a shuttle mass of 160 ng, this energy storage translates into a final shuttle velocity of 15.4 m/s, or about 34 mph. If we also assume that only 50% of the energy is transferred when the shuttle impacts a small projectile, then the projectile will have about 9.5 nJ of kinetic energy, which, for a 10 ng projectile corresponds to about 43.6 m/s, or about 97.5 mph. Actual images of the system in an energized state are shown in figure 12.

Device Properties					
E	I	L	r_1	e	r_3
168 GPa	12.8 μm⁴	131.4 μm	346.8 μm	74.1 μm	393.4 μm

Table 1. Device properties used in evaluating Equations (1) through (5).

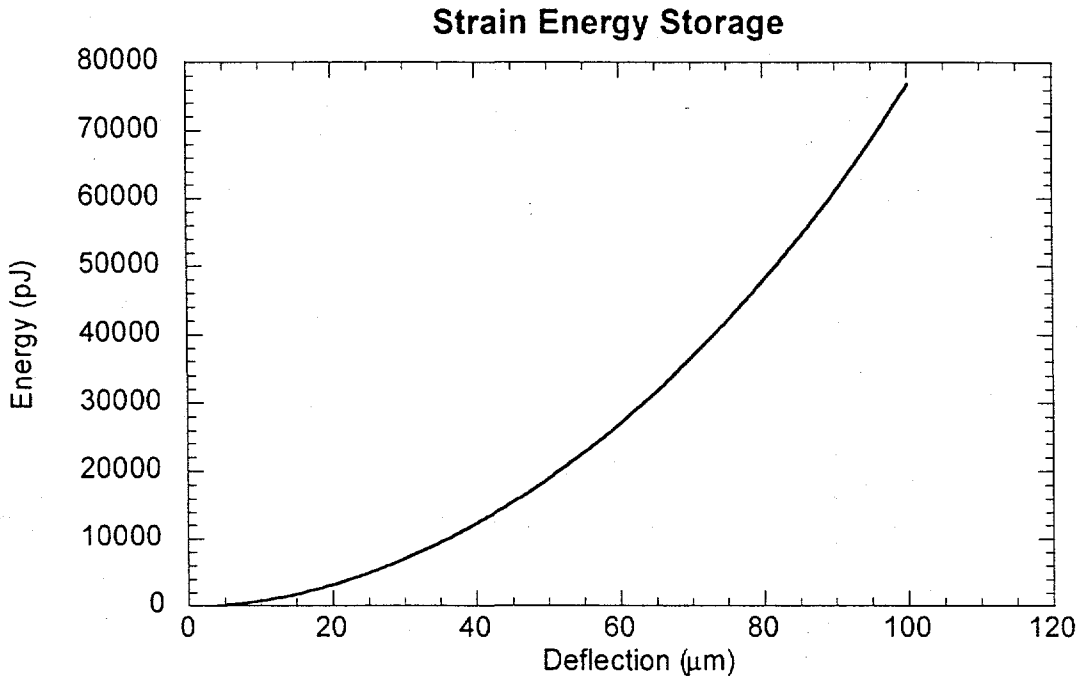

Figure 10. Energy stored in the device as a function of deflection δ.

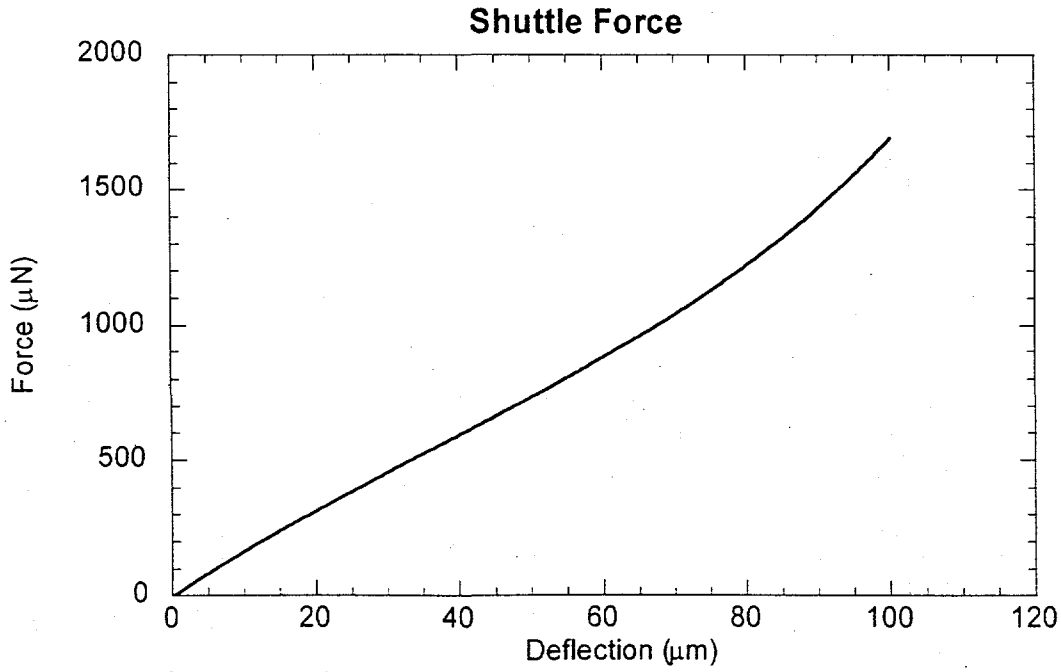

Figure 11. Force required to deflect the shuttle as a function of deflection.

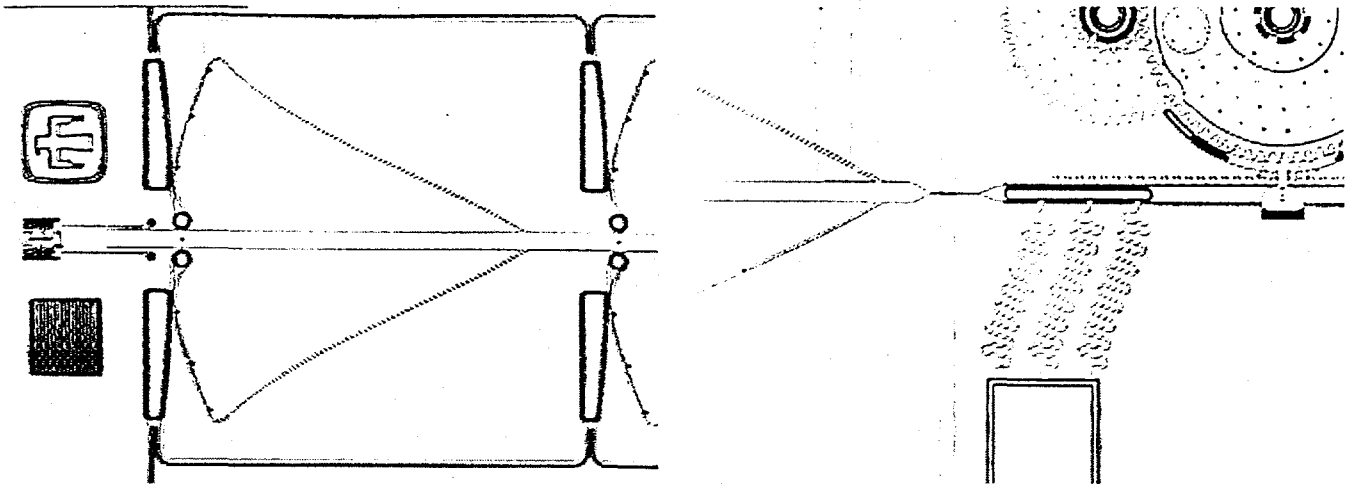

Figure 12. Optical images extracted from a digital movie clip of the system in an energized state. The bowed cantilever beams are displayed on the left. The filament that connects the central beam to the rack can be seen on the right along with the triple set of compliant springs that carry the current while blowing the filament.

9. CONCLUSIONS

This paper clearly demonstrates that significant work can be derived from low-power surface micromachined electrostatic actuation systems. However, almost any actuator that could drive a gear or even directly pull on the rack could be utilized in a similar device. This high density energy storage / rapid release system opens up many new potential applications for MEMS. In some sense, our original goal of determining how much force could be obtained from a microengine assisted with the modular gear reduction units was not achieved because the energy storing mechanical load is insufficient to fully stress the actuation system. Therefore, systems with stronger energy storage springs are being developed. We are also investigating the benefit of using high-voltage electrostatic assist to deliver even more energy to the load.

ACKNOWLEDGEMENTS

The authors are grateful to the personnel of the Microelectronics Development Laboratory at Sandia National Laboratories for fabricating these devices and to Gary Zender for the excellent SEM images.

Sandia is a multiprogram laboratory operated by Sandia Corporation, a Lockheed Martin Company, for the United States Department of Energy under Contract DE-AC04-94AL85000.

REFERENCES

1. M. Steven Rodgers, Samuel L. Miller, Jeffry J. Sniegowski, and Glenn F. LaVigne, "Designing and Operation Electrostatically Driven Microengines", Proceedings of the 44th International Instrumentation Symposium, 5/3-7/98, Reno, Nevada, pp. 56-65.
2. Additional information may be found on the web at http://www.mdl.sandia.gov/Micromachine.
3. J. J. Sniegowski and M. S. Rodgers, "Multi-layer enhancement to polysilicon surface-micromachining technology", IEDM97, 12/7-10/97, Washington DC, pp. 903-906.
4. S. L. Miller, J. J. Sniegowski, G. LaVigne, and P. J. McWhorter, "Friction in surface micromachined microengines", *Proc. SPIE Smart Electronics and MEMS*, 2722, 2/28-29/96, San Diego, CA, pp. 197-204, 1996.
5. W. C. Tang, Ph.D. Thesis, University of California, Berkeley, CA. (1990).
6. L. Que, J.-S. Park, and Y. B. Gianchandani, "Bent-Beam Electro-Thermal Actuators For High Force Applications," IEEE Micro Electro Mechanical Systems Technical Digest 1999, 1/17-21/99, Orlando, Florida, pp. 31-36.
7. M. S. Rodgers and J. J. Sniegowski, "5-Level Polysilicon Surface Micromachine Technology: Application To Complex Mechanical Systems", *1998 Solid State Sensor and Actuator Workshop*, Hilton Head Island, SC, 6/8-11/98, pp. 144-149.

8. M. Steven Rodgers, Jeffry J. Sniegowski, James J. Allen, Samuel L. Miller, James H. Smith, and Paul J. McWhorter, "Intricate Mechanisms-on-a-Chip Enabled By 5-Level Surface Micromachining," The 10th International Conference on Solid-State Sensors and Actuators, Sendai, Japan, 6/7-10/99.
9. E. J. Garcia and J. J. Sniegowski, "Surface Micromachined Microengine as the Driver for Micromechanical Gears", *Proc. of the 8th International Conf. on Solid-State Sensors and Actuators and Eurosensors IX,* 6/25-29/95, Stockholm, Sweden 1, pp. 365-368.
10. J. J. Sniegowski and E. J. Garcia, "Microfabricated Actuators and Their Application to Optics", *Proc. SPIE Miniaturized Systems with Micro-Optics and Micromechanics, 2383*, 2/7-9/95, San Jose, CA, (1995) pp. 46-64.
11. S. L. Miller, G. LaVigne, M. S. Rodgers, J. J. Sniegowski, J. P. Waters, and P. J. McWhorter, "Routes to failure in rotating MEMS devices experiencing sliding friction", *Proc. SPIE Micromachined Devices and Components III,* 3224, 9/29/97, Austin, TX, pp. 24-30.
12. J. J. Sniegowski, S. L. Miller, G. LaVigne, M. S. Rodgers, and P. J. McWhorter, "Monolithic Geared Mechanisms Driven by a Polysilicon Surface Machined On-chip Electrostatic Engine", *Technical Digest of the 1996 Solid State Sensor and Actuator Workshop,* Hilton Head Island, SC, 6/3-6/96, pp.178-182.
13. S. L. Miller, J. J. Sniegowski, G. LaVigne, and P. J. McWhorter, "Performance Tradeoffs for a Surface Micromachined Microengine", *Proc. SPIE Micromachined Devices and Components II*, 2882, 10/14-15/96, Austin, TX, pp.182-191.
14. D. W. Dudley, "Handbook of Practical Gear Design," McGraw-Hill Book Company, 1984, pp. 3.8-3.9.
15. Howell, L.L. and Midha, A., "Parametric Deflection Approximations for End-Loaded, Large-Deflection Beams in Compliant Mechanisms," *ASME Journal of Mechanical Design*, Vol. 117, No. 1, 1995, pp. 156-165.
16. Howell, L.L, Midha, A., and Norton, T.W., "Evaluation of Equivalent Spring Stiffness for Use in a Pseudo-Rigid-Body Model of Large-Deflection Compliant Mechanisms," *ASME Journal of Mechanical Design*, Vol. 118, No. 1, 1996, pp. 126-131.